Electrocatal (2012) 3:13–21
DOI 10.1007/s12678-011-0071-0

Carbon-Supported Silver as Cathode Electrocatalyst for Alkaline Polymer Electrolyte Membrane Fuel Cells

Subbiah Maheswari · Parthasarathi Sridhar · Sethuraman Pitchumani

Published online: 21 September 2011

Abstract Carbon-supported silver in varying percentage viz. 40%, 60%, and 80% (Ag/C) is prepared by sodium citrate protecting method. The structure, dispersion, electrochemical characterization, and surface area and oxygen reduction reaction pathway of Ag/C are determined by XRD, TEM, CV, and LSV, respectively. The catalyst is evaluated for its electrocatalytic activity towards oxygen reduction reaction (ORR) in alkaline polymer electrolyte membrane fuel cells (APEMFCs); 60% Ag/C gives higher performance than 40%, and 80% Ag/C. Metal loading on cathode is optimized through the cell polarization studies using 60% Ag/C. A peak power density of 10 mW/cm^2 is obtained for APEMFC single cell comprising 60% Ag/C and 38% Pt/C as cathode and anode catalysts, respectively.

Keywords Alkaline polymer electrolyte membrane fuel cell · Electrochemical surface area · Tafel slope · Oxygen reduction reaction · Carbon-supported silver

Introduction

Polymer electrolyte membrane fuel cells (PEMFCs) and alkaline fuel cells (AFC) are the most attractive low temperature fuel cells due to their high power densities but their commercialization is still inhibited by high cost of the electrocatalyst and highly corrosive liquid electrolyte, respectively. Alkaline polymer electrolyte in PEMFC is being explored to overcome the aforesaid problems. PEMFCs using alkaline polymer membrane as electrolyte are referred to as alkaline polymer electrolyte membrane fuel cells (APEMFCs); a schematic diagram of the same is shown in Fig. 1. APEMFCs have many advantages over PEMFCs, viz. usage of non-precious metal catalyst, less corrosive, decreased cathodic overpotential and favorable water management. Among these, one of the most attractive advantages of APEMFCs is the possibility to replace Pt-based electro catalyst with cheaper non-Pt electrocatalysts for both electrodes [1, 2]. In fuel cells, cathodic reaction (oxygen reduction reaction-ORR) is very interesting and challenging due to its complicated pathway compared to hydrogen oxidation.

It is desirable to have as a cathode catalyst one that would meet the following requirements viz. (a) good oxygen adsorption capacity, (b) structural stability towards oxygen adsorption and desorption, (c) stability in electrolyte medium, (d) efficient breaking of oxygen bonds, (e) ability to decompose hydrogen peroxide, (f) good conductivity and (g) affordable cost [3]. The above criteria are satisfied by Pt-group metals and Ag as the ORR catalysts especially for alkaline medium. The activity of the Pt-group metals for ORR is very high, and some of the most successful catalysts to date (such as Pt/Au cathodes used in the space shuttle) have contained Pt-group metals. However, Pt suffers from slow dissolution in alkaline electrolyte and therefore its stability has been a serious concern [4]. Ag shows ORR activity close to that of Pt [5, 6]. Hence, Ag is a common cathode electrocatalyst in alkaline fuel cell. The degree of surface oxidation of Pt increases with increasing pH. This surface oxidation inhibits ORR kinetics. In contrast, Ag, which has a completely filled *d* band, is much less oxophilic than Pt, so surface oxidation is not a significant factor [7]. Voltammetric studies for Ag catalyst reported in alkaline medium are found to proceed via a

S. Maheswari · P. Sridhar (✉) · S. Pitchumani
CSIR—Central Electrochemical Research Institute, Madras Unit, CSIR Complex,
Chennai 600 113, India
e-mail: psridhar55@gmail.com

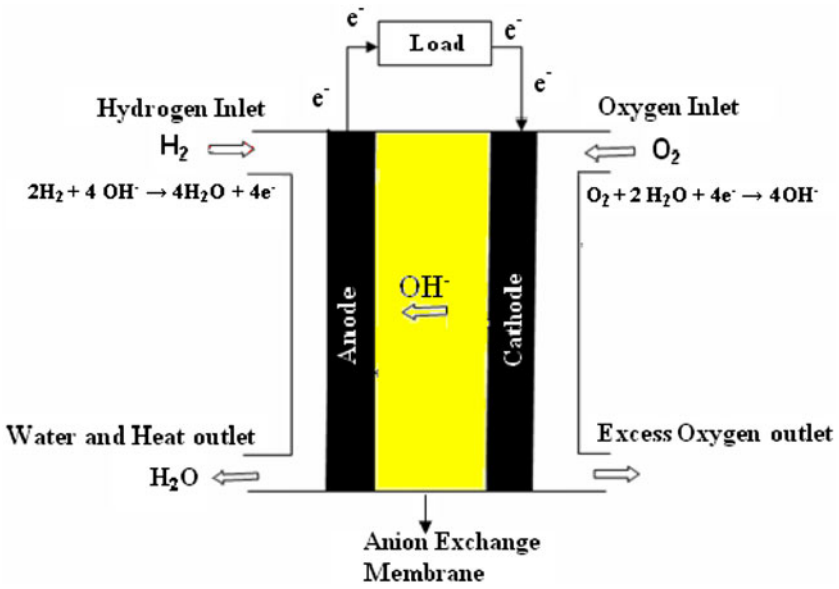

Fig. 1 Schematic diagram of APEMFC

four-electron transfer step with very little production of undesirable H_2O_2 [8]. Hence, Ag is stable in highly concentrated alkaline medium and competitive to Pt.

Silver also has some additional benefits over platinum. The cost is 1/70th the price of platinum, it is half the density of platinum, with the same mass loading, more Ag particles are formed compared to Pt and thus the surface area will be larger and it may not suffer from a particle size effect to the same extent as platinum [9]. Hence, Ag is the best one to replace Pt for ORR in alkaline solution due to its high electrocatalytic activity, better stability, low oxophilicity, low cost, and abundance. Additionally, it is a good catalyst for hydrogen peroxide decomposition [10].

Coutanceau et al. have shown by linear sweep voltammetry (LSV) studies on ORR that 20% Ag/C exhibits better catalytic activity than 30% and 40% Ag/C [11]. But Varcoe et al. have reported that the performance of 60% Ag/C with a loading of 4 mg cm^{-2} is comparable to that of 20% Pt/C with a loading of 0.5 mg cm^{-2} in APEMFCs [12]. Park et al. have shown better performance with 2 mg cm^{-2} loading compared to the one with 1 and 0.5 mg cm^{-2} while using 40% Ag/C [13].

Han et al. reported that 20% Ag/C with an average particle size of 174 and 4.1 nm show four- and two-electron transfer, respectively, for oxygen reduction reaction [14]. Guo et al. investigated the effect of metal loading of carbon-supported Ag in half-cell mode and showed that 60% Ag/C has better kinetic activity than 10%, 20%, and 40% [15]. Wiberg et al. have obtained the charge density of nanoparticle and polycrystalline silver using the underpotential deposition method [16].

The above-presented literature forms the basis for the present study on the need for comparative evaluation of the performance pertaining to ORR in half-cell as well as in fuel cell mode with reference to Ag loading on carbon support, particle size, surface area, and catalyst loading on the electrode.

In the present study, varying silver loading on carbon is prepared by sodium citrate protecting method. The structure and particle size of catalysts were characterized by X-ray diffraction (XRD) and transmission electron microscopy (TEM), respectively. Electrochemical surface area was determined for the prepared catalysts and their catalytic activities for ORR in alkaline medium were investigated. Catalysts were evaluated by the polarization studies and the metal loading on the electrode was also optimized for APEMFCs.

Experimental section

Preparation of catalyst

Procedure for preparation of silver on carbon support by citrate protecting method reported in the literature was followed [15, 17]. In brief, for preparation of 1 g of 40% of Ag/C catalysts, 0.629 g of $AgNO_3$ (Rankem) was dissolved in deionized water followed by the addition of 35 ml of 0.5 M tri sodium citrate (Merck) for the formation of silver citrate as white precipitate. The role of sodium citrate is to prevent the agglomeration of the metallic particles during the reduction step and allow the formation of nanoparticles [11]. Carbon (0.6 g; Vulcan XC72 R) was sonicated for 30 min and added to the silver citrate containing solution. To this, 50 ml of 0.5 M alkaline $NaBH_4$ was added drop by drop and maintained under ice-cold condition. After the addition of $NaBH_4$, the suspension was stirred for 1 h, filtered and washed until reaching a neutral pH, and dried in a vacuum oven at 80 °C overnight.

Physical Characterization

Powder XRD studies were conducted to analyze the crystallinity of carbon-supported Ag nanocatalyst. For this purpose, powder XRD patterns were obtained on a Philips X'Pert Diffractometer using CuKα radiation (λ=1.5406 Å) between 20° and 80° in reflection geometry in steps of 0.017º/s.

TEM was used to determine the average particle size and dispersion of carbon-supported Ag catalysts. For this purpose, the microscopic features of the samples were examined by using TCNAI 20 G2 transmission electron microscope (200 kV). For TEM characterization, a carbon film deposited onto a mica sheet that was placed onto the copper grid was used. Catalyst was suspended in isopropyl alcohol and cast by dropping the suspension onto a carbon-coated copper grid followed by solvent evaporation in vacuum at room temperature (~25 °C).

Electrochemical Characterizations

Cyclic Voltammetry and Linear Sweep Voltammetry

Ag/C catalysts were electrochemically characterized using cyclic voltammetry (CV) and ORR was evaluated based on the LSV measurements with three-electrode configuration using a computer-controlled electrochemical analyzer (Autolab PGSTAT-30). A conventional three-electrode cell consisting of glassy carbon (GC) disk with a geometric area of 0.071 cm^2 was used as the working electrode. Before each test, the electrodes were polished with 0.06 μm alumina on a polishing cloth to obtain a mirror-like finish followed by rinsing with double-distilled water in an ultrasonic bath. To prepare the working electrode, catalyst (40% or 60% or 80% Ag/C) suspension of 35.5 $\mu g_{Ag}/cm^2$ with 10% Nafion (Dupont) was quantitatively transferred to the surface of polished GC disk. In this case, Nafion helps to attach the catalyst particles on the GC electrode [18]. The electrode was dried at room temperature. A pre-calibrated mercury-mercuric oxide (MMO, 0.160 V vs. NHE) electrode and a Pt foil were used as the reference and counter electrodes, respectively, in the three-electrode configuration. All electrochemical experiments were carried out at room temperature (~25 °C).

In order to clean and activate the working electrode, it was cycled between−0.9 and 0.5 V with respect to MMO at a sweep rate of 50 mV/s in high pure-nitrogen-purged 1 M KOH, until stable and reproducible voltammograms were obtained. The cyclic voltammograms were recorded once the working electrode was well equilibrated. LSV experiments were performed using rotating disk electrode (RDE) in oxygen-saturated 1 M KOH. LSV data were recorded in the negative-going sweep direction from 0.2 V to −0.6 V vs. MMO over a range of rotations (400 to 2,400 rpm) at a scan rate of 3 mV/s.

Fuel cell studies

Customizing the Electrolyte and Preparation of Ionomer

Ammonium-type anion exchange membrane (AHA-Neosepta) was modified from Cl^- to OH^- form as follows. The AHA membrane comprised tetra-alkyl ammonium groups as fixed cation groups bonded to a polyolefin backbone chain. The Cl^- form membrane was rinsed several times with deionized water, and then immersed in 4 mol dm^{-3} KOH aqueous solution at room temperature overnight for the replacement of Cl^- with OH^-. The membranes were again washed several times with deionized water at room temperature. OH^- form AHA membrane was dissolved in ethanol using an autoclave to make an (0.05 N) ionomer solution.

Fabrication of Membrane Electrode Assembly (MEA)

Membrane electrode assembly (MEA) preparation for APEMFCs was already described elsewhere [18]. In brief, both electrodes comprised backing layer, gas-diffusion layer and catalyst layer. For backing layer, carbon paper (Toray TGP-H-120) of 0.35 mm thickness was teflonized with 15 wt. % of polytetrafluoroethylene (PTFE) emulsion and sintered at 350 °C for 1 h. The gas-diffusion layer was coated with a homogeneous suspension of high surface area carbon (Vulcan XC72 R) with 1.5 mg cm^{-2} loading over the teflonized Toray sheet, which was then sintered at 350 °C for 0.5 h.

To prepare the catalyst layer, 44.2 mg of 38% Pt/C (Johnson Matthey Corp.), as anode catalyst or Ag/C as cathode catalyst was suspended in isopropyl alcohol. The mixture was agitated in an ultrasonic water bath, and 15 wt.% of PTFE emulsion that acts as a binder was added to the solution. 1.5 ml of anion conducting ionomer was added only to the cathode slurry with continuous ultrasonication [18]. The resulting ink was coated on a gas-diffusion layer. Both anode and cathode contained a catalyst loading of 0.5 mg cm^{-2} (active area 25 cm^2) which was kept identical in all the MEAs. MEAs were obtained by pressing the cathode and anode on either side of the anion exchange membrane under a compaction pressure of 60 kg cm^{-2} at room temperature for 5 min.

Cell Polarization Studies

The performance of MEAs was evaluated using a conventional 25-cm^2 fuel cell fixture with a parallel serpentine flow field machined on graphite plates (Schunk Kohlenstofftechnik GmbH, Germany). After equilibration, the single cells were tested at room temperature (30 °C) with humidified hydrogen and oxygen at anode and cathode, respectively at a flow rate of 0.5 L/min at atmospheric pressure. Measurements of cell potential as a function of

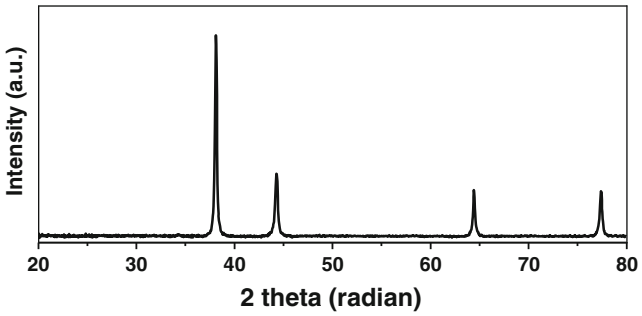

Fig. 2 XRD pattern of 60% Ag/C

current density were conducted potentiostatically using a LCN10-40 electronic load procured from Bitrode Corporation.

Results and Discussion

The crystalline structures of three different metal loadings of Ag/C catalyst were characterized by XRD and the observed patterns for the catalysts are similar. A typical XRD pattern obtained for 60% Ag/C is shown in Fig. 2. The diffraction peaks at 2θ values of 38.04º, 44.38º, 64.54º and 77.4º are due to the (111), (200), (220), and (311), respectively for the

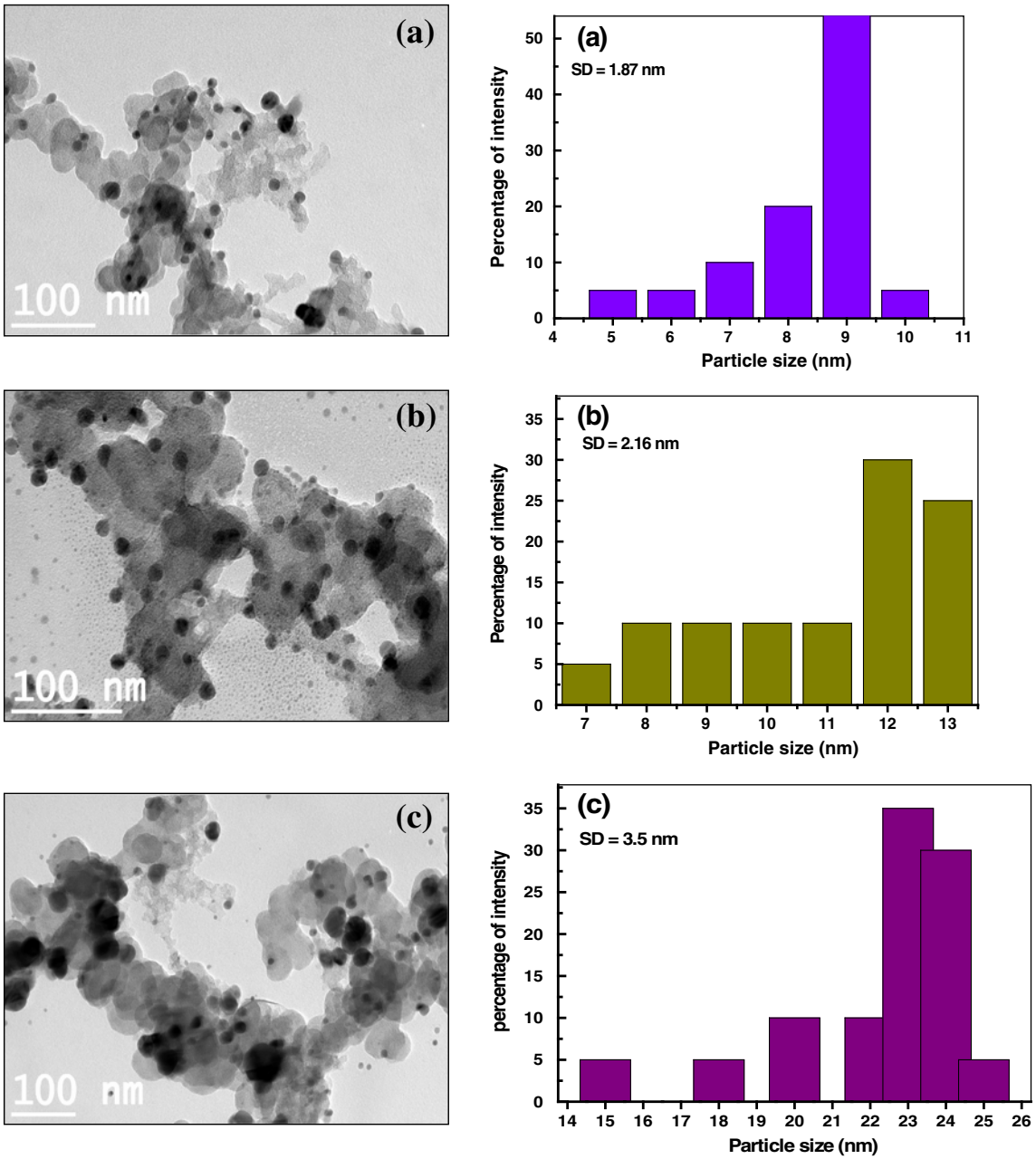

Fig. 3 TEM images and the corresponding particle size distribution histograms for **a** 40% **b** 60%, and **c** 80% Ag/C

crystalline planes of Ag with a face-centered cubic structure in conformity with The American Mineralogist Crystal Structure Database (AMCSD 0013118). The XRD pattern indicates that the silver particles present in the carbon-supported Ag catalysts are in metallic form since no characteristic peak of oxide is found.

The TEM images of 40%, 60%, and 80% Ag/C catalysts are shown in Fig. 3. The silver nanoparticles are well dispersed on the surface of carbon and the particles are spherically shaped and are of similar size. The mean particle diameter (d) calculated using the formula $d = \frac{(\sum_i n_i d_i)}{(n_i)}$, where n_i is the frequency of occurrence of particles of dia, d_i, i.e. 9.01, 12.66 and 23.98 nm for 40%, 60%, and 80% Ag/C, respectively. It is to be noted that typically a particle size of 13.9 nm is reported for 40% Ag/C while only 9.01 nm is observed in the present study probably due to the ice-cold condition under which the preparation is carried out. In this study, the mean size of the silver nanoparticles on carbon support is obtained by measuring 200 randomly chosen particles in the magnified TEM images. The standard deviation for the particle size of 40%, 60%, and 80% Ag/C are 1.87, 2.16, and 3.5 nm respectively and with increased Ag loading, the particle size increases which may be due to agglomeration.

The cyclic voltammograms of Ag/C catalysts in freshly prepared 1 M KOH solution purged with nitrogen are shown in Fig. 4. There are three anodic peaks, namely, A_1, A_2, and A_3 appearing at 0.16, 0.24 and 0.31 V vs. MMO, respectively and one cathodic peak, C_1 appearing at 0.1 V vs. MMO in good agreement with that reported [15]. The anodic peaks appearing between 0.16 and 0.35 V vs. MMO are due to the formation of Ag_2O layers and the cathodic peak at 0.1 V vs. MMO is assigned to the reduction of

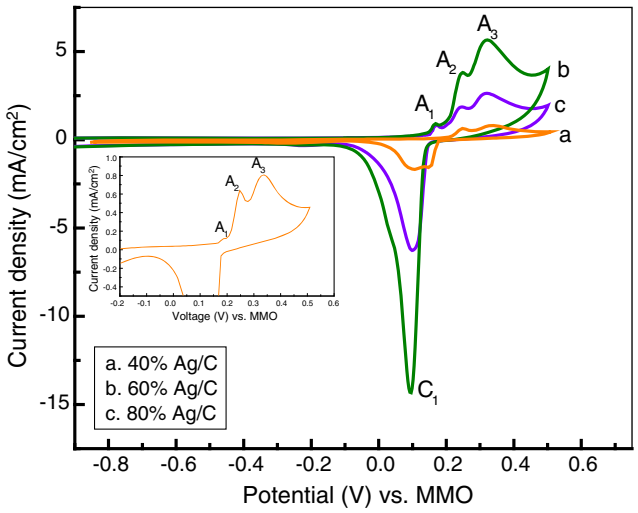

Fig. 4 Cyclic voltammograms of **a** 40%, **b** 60%, and **c** 80% Ag/C in deaerated 1.0 M KOH at a sweep rate of 50 mV/s. *Inset* expanded anodic peaks of CV of 40% Ag/C

Ag_2O back to metallic silver form. According to Chen et al. [19], peak A_1 is due to silver dissolution and formation of surface monolayer of Ag_2O film while peaks A_2 and A_3 are due to the formation of AgOH and Ag_2O, respectively and AgOH, the short-lived intermediate, is the transition form of Ag_2O. However, Jovic et al. have interpreted the peaks A_2 and A_3 as due to compact and porous Ag_2O layer, respectively [20]. One cathodic peak, the counterpart of the three anodic peaks, C_1, due to reduction of Ag_2O to Ag form is observed in the following negative sweep.

In the present study, the potential window was limited to +0.5 V vs. MMO. It is recorded in the literature that if the scan is carried beyond +0.5 V vs. MMO, AgO would deposit on the Ag_2O [20, 21]. If AgO were present during negative sweep, this would reduce to form Ag_2O and subsequently Ag_2O would reduce to Ag [22]. In the present case, it is conjectured based on the observation of two peaks, one at 1.78 V vs. MMO and the other one at 1.5 V vs. MMO for 40% Ag/C and a shoulder for the 60% Ag/C that the reduction of AgO to Ag takes place via Ag_2O, keeping in view that the reduction potential of AgO is higher than that of Ag_2O [22]; 60% Ag/C shows high current density in relation to 40% and 80% Ag/C as shown in Fig. 4.

Linear sweep voltammograms are obtained at various rotation rates namely, 400, 800, 1,200, 1,600, 2,000, and 2,400 rpm and the current density (normalized in reference to geometric area of working electrode) increased with increase in rotation rate for 40%, 60%, and 80% Ag/C catalysts as shown in Fig. 5a, b and c, respectively.

Figure 5d shows the rotation rate dependence of the three carbon-supported silver (40%, 60%, and 80%) in oxygen-saturated 1 M KOH solution at a rotation rate of 1,600 rpm and at a scan rate of 3 mV/s. At higher rotation rates, the effect of mass transport decreases compared to the lower rotation rates [23].

In Fig. 5d, a peak observed at 0.15 V vs. Hg/HgO is due to the reduction of Ag(I) to Ag(0), i.e. Ag_2O to Ag [22].

$$Ag_2O + H_2O + 2e^- \rightarrow 2Ag + 2OH^- \quad (1)$$

The oxide reduction peak is used to determine the electrochemical surface area (ESA). Unlike platinum, ESA of Ag/C could not be determined using CV for lack of adsorption of hydrogen. Therefore the ESA is calculated from the charge corresponding to the reduction of oxide, which is formed due to adsorption of monolayer of oxygen [24].

$$\mathrm{ESA}\left(\mathrm{cm}^2/\mathrm{mg}_{\mathrm{Ag}}\right) = \frac{Q_{\mathrm{O}}(\mu\mathrm{C}/\mathrm{cm}^2)}{420\mu\mathrm{C}/\mathrm{cm}^2 \times \mathrm{electrodeloading}\left(\mathrm{mg}_{\mathrm{Ag}}/\mathrm{cm}^2\right)} \quad (2)$$

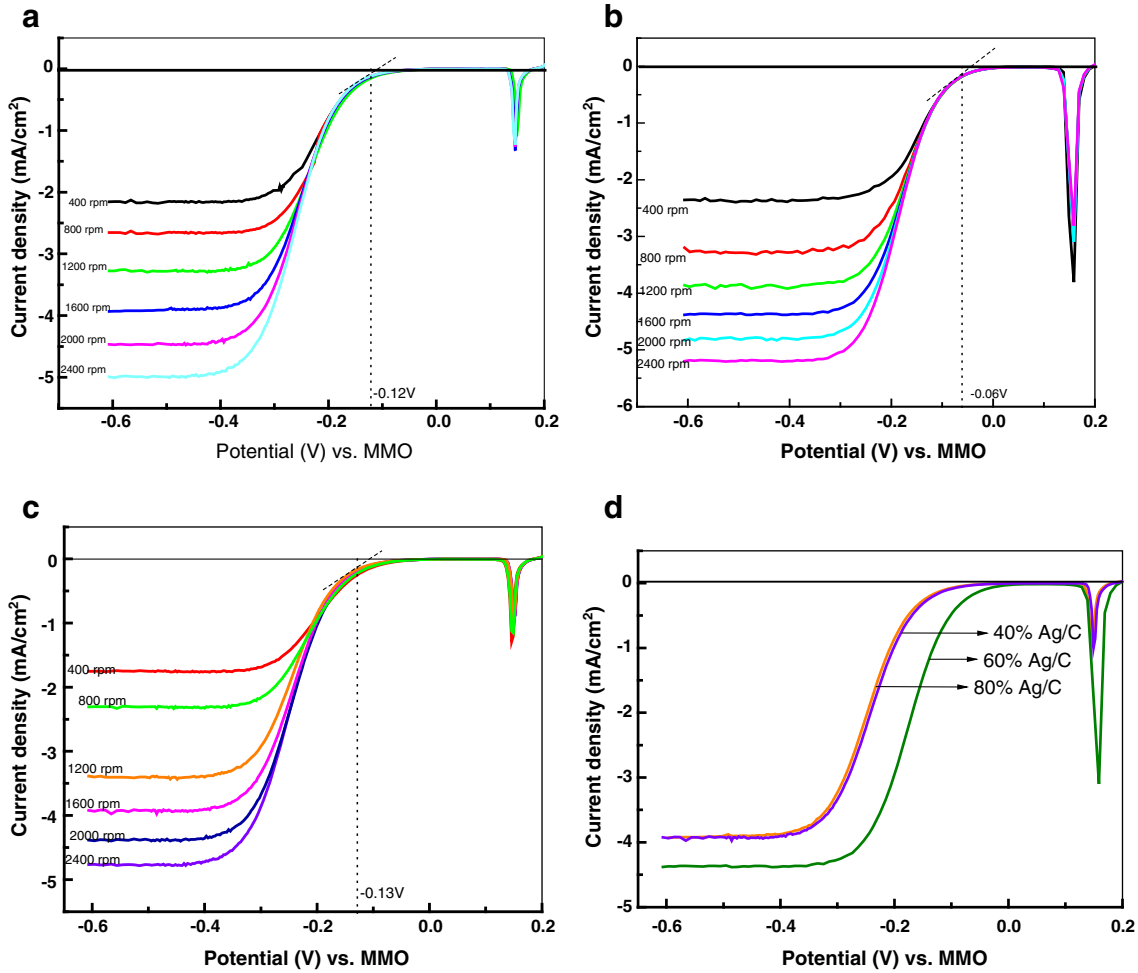

Fig. 5 Linear sweep voltammograms of **a** 40%, **b** 60%, **c** 80% Ag/C in oxygen-saturated 1.0 M KOH at vaious rotation rates and **d** comparative LSV of 40%, 60%, and 80% Ag/C in oxygen-saturated 1 M KOH solution at 1600 rpm

Q_O, the charge of monolayer of oxygen is twice that of the hydrogen monolayer Q_H on platinum. The ESA of 40%, 60%, and 80% of Ag/C are 75, 88.8, and 69 m^2/g, respectively. ESA of 60% is higher than that of 40% and 80% of Ag/C. Mass activities of these catalysts are calculated using the ESA values obtained and 60% Ag/C has higher mass activity than 80% and 40% Ag/C; 60% Ag/C shows 60 mV and 70 mV higher onset potential for ORR in relation to 40 and 80% Ag/C, respectively. Half-wave potential for ORR on 40%, 60%, and 80% Ag/C are, −0.251, −0.175, and−0.247 V, respectively. It is clear from the values of ESA, onset potential, and half-wave potential values for ORR that 60% Ag/C has higher electrocatalytic activity compared to 40 and 80% Ag/C (Table 1).

The number of electron transfer and order of reaction may help to understand the catalytic activity of Ag/C. The electrochemical reduction of oxygen is a multi-electron reaction and it has two main possible pathways. One is an indirect four-electron transfer process, which produces hydrogen peroxide as an intermediate while the other is a direct four-electron transfer process producing hydroxyl ion as the final product [25]. The RDE method provides

Table 1 Kinetic parameters derived from hydrodynamic polarization curves of ORR

Catalyst% Ag/C	Onset potential (mV)	Kinetic current density (mA/cm^2)			Mass activity at −0.1 V vs. MMO (mA/g_{Ag})	Half-wave potential ($E_{1/2}$) (mV)	Tafel slope value (mV/dec)	No. of electron transfer
		at −0.1 V	at −0.2 V	at −0.3 V				
40	−120.0±0.2	0.053±0.002	1.024±0.002	4.207±0.002	39.75±0.08	−250.0±0.5	82±1	3.9
60	−60.0±0.1	0.380±0.002	1.460±0.002	6.666±0.002	337.44±0.67	−170.0±0.3	78±1	4
80	−130.0±0.3	0.106±0.002	1.135±0.002	4.923±0.002	73.14±0.14	−240.0±0.5	80±1	3.7

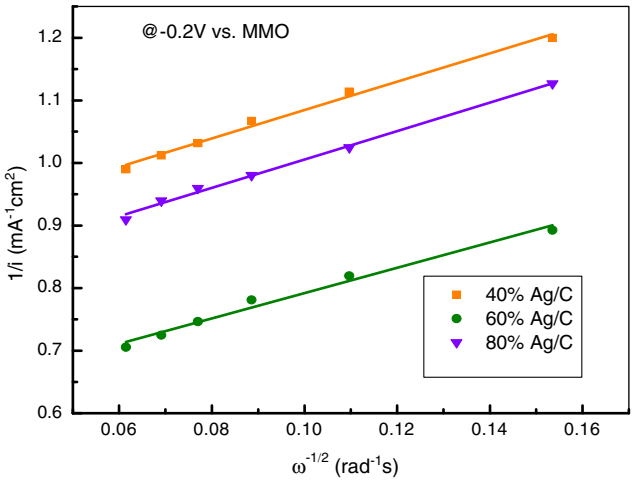

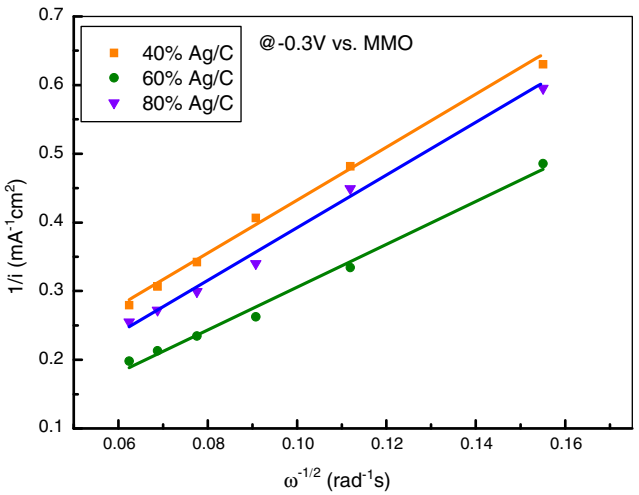

Fig. 6 K–L plots at −0.2 and −0.3 V vs. MMO of different revolutions per minute

continuous supply of oxygen to the electrode surface facilitating the determination of catalytic activity free of diffusion limitation.

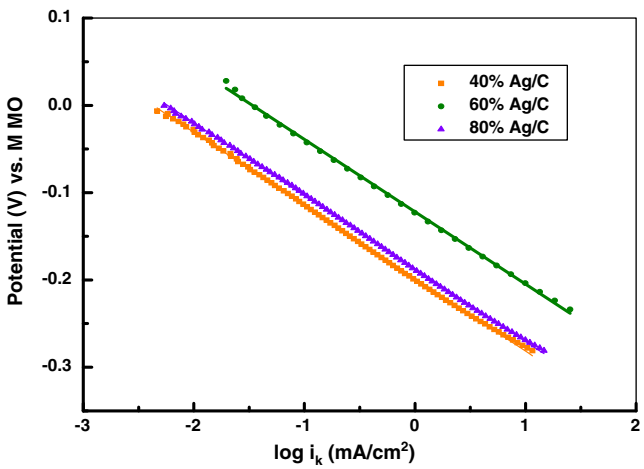

Fig. 7 Tafel plots of **a** 40%, **b** 60%, and **c** 80% Ag/C for ORR

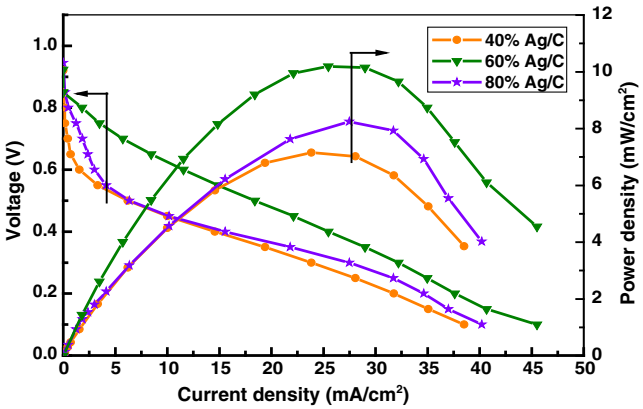

Fig. 8 Steady-state performance curves for APEMFCs comprising 40%, 60%, and 80% Ag/C as cathode catalyst at room temperature

The number of electron transfer (n), can be obtained from the slope of Levich plots under diffusion limiting conditions using the following equation,

$$i_{\mathrm{d}} = 0.62nFAC_{\mathrm{o}}D_{\mathrm{o}}{}^{2/3}\upsilon^{-1/6}\omega^{1/2} \tag{3}$$

in short form of Eq. 3,

$$i_d = B\omega^{1/2} \tag{4}$$

Where

$$B = 0.62\,nFAC_{\mathrm{o}}D_{\mathrm{o}}{}^{2/3}\upsilon^{-1/6} \tag{5}$$

B is the Levich slope. n is the number of electrons involved in the ORR per oxygen molecule, F is the Faraday constant (96,486 C mol^{-1}), A is the surface area of electrode (0.071 cm^2), C_{o} is the saturation concentration of oxygen in 1 M KOH (0.84×10^{-3} mol L^{-1}) [26, 27], D_{o} is the diffusion coefficient of O_2 in 1 M KOH solution (1.4×10^{-5} cm^2 s^{-1}) [28], ν is the kinematic viscosity of the solution (0.01 cm^2 s^{-1}) [29] and ω is the rotation rate in revolutions

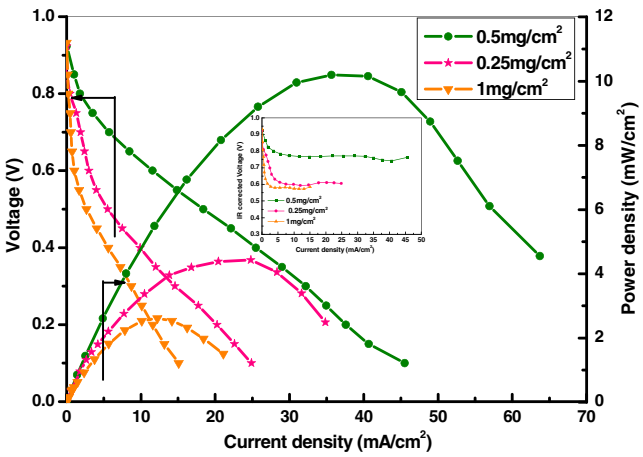

Fig. 9 Steady-state performance curves for APEMFCs comprising cathode with varying Ag loading (0.25, 0.5, and 1 mg/cm^2) of 60% Ag/C at room temperature. *Inset* IR-corrected performance curve

per second. Generally, under the mass-transfer-limiting condition, the Levich slope is constant. However, in this study, when cathodic-limiting current densities are plotted vs. $\omega^{1/2}$, a slightly curved line (not shown) is observed. Hence, in order to eliminate the kinetic influence, the Koutecky–Levich (K–L) plots based on K–L equation viz.

$$1/i = 1/i_k + 1/i_d \tag{6}$$

$$1/i = 1/i_k + 1/\left(B\omega^{1/2}\right) \tag{7}$$

are drawn. A plot of $1/i$ (at −0.2 and −0.3 V vs. MMO) vs. $1/\omega^{1/2}$ as shown in Fig. 6 is linear and on extrapolation to $\omega^{-1/2}=0$ yields $1/i_k$ [30]. It is clear from Table 1 that 60% Ag/C catalyst shows enhanced kinetic current–density (i_k) in relation to 40% and 80% of Ag/C. From the slope of K–L plots (B), the value of n is calculated to be nearly 4 for both 40% and 60% Ag/C catalyst indicating that ORR proceeds through a direct four-electron pathway unlike 80% Ag/C in which case n is around 3.7. Though in a typical case, i.e., at 1,600 rpm the limiting current for 40% and 80%Ag/C are the same, it is not the case at all revolutions per minute. Hence, there is a difference in the n value when it is obtained from the slope of i^{-1} vs. $\omega^{-1/2}$. A value less than 4 obtained for number of electrons could be explained based on the fact that although predominance of the four-electron pathway during ORR on Ag is widely acknowledged, peroxide formation as an intermediate in the four-electron pathway may not be completely eliminated [31]. Even with Pt/C as electrocatalyst, ~1% of peroxide is reported to have been produced [32]

The electrocatalytic activity for ORR in the different ultra thin layer electrodes can be more adequately compared in terms of mass transport corrected Tafel plot [23]. Figure 7 is the Tafel plot for normalized kinetic current with respect to potential, wherein the former is derived using the following equation

$$i_k = (i_d \times i)/(i_d - i) \tag{8}$$

and the only one linear plot obtained clearly shows that the ORR conforms to only one isotherm and also 60% Ag/C shows higher catalytic activity in relation to 40% and 80% Ag/C. The Tafel slopes obtained at low overpotential (i.e., $-0.1<E<0$) from the above plot are given in Table 1. It is interesting to note that the Tafel values obtained are in agreement with that reported in the literature [8, 23]. It is also interesting to note that ESA, onset potentials, kinetic currents, mass activities, half-wave potentials, and Tafel slopes, clearly reveal that 60% Ag/C is a better electrocatalyst than 40% and 80% Ag/C.

Steady-state polarization studies are conducted for APEMFCs comprising 40%, 60%, and 80% Ag/C as cathode catalyst and 38% Pt/C as anode catalyst at room temperature. For polarization studies, hydrogen and oxygen (H_2/O_2) were used as fuel and oxidant respectively. Figure 8 shows steady-state performance curves for APEMFCs with 40%, 60%, and 80% Ag/C as cathode catalysts. Among the various APEMFCs, the cell comprising 60% Ag/C shows higher peak power density of 10 mW/cm^2 in relation to 40% Ag/C (7.5 mW/cm^2) and 80% Ag/C (8 mW/cm^2), respectively. The polarization values are found to corroborate well with the trend observed in the kinetic studies.

In order to optimize the catalyst loading, APEMFCs with varying cathode catalyst loading viz., 0.25, 0.5, and 1 mg/cm^2 of 60% Ag/C are evaluated. Figure 9 shows the steady-state performance of APEMFCs with varying cathode catalyst and 0.5 mg/cm^2 Pt/C anode catalyst while employing H_2/O_2. APEMFC with 0.5 mg/cm^2 cathode catalyst loading shows enhanced performance in relation to that with 0.25 and 1 mg/cm^2 as cathode catalyst. The reduced performance in case of APEMFC with a catalyst loading of 1 mg/cm^2 may be due to increased ohmic polarization on account of the increased Teflon content in the catalyst layer which was kept in proportion to the metal loading to take care of effective binding of the particles in the catalyst layer besides reduced availability of active sites at the interface, while that in the case of APEMFC with a catalyst loading of 0.25 mg/cm^2 may be attributed to the insufficient active catalyst sites for oxygen reduction reaction. Thus, APEMFC comprising cathode with a metal loading of 0.5 mg/cm^2 of 60% Ag/C shows better performance of 10 mW/cm^2.

Conclusions

A percentage of 60% Ag/C shows enhanced performance in relation to 40% and 80% Ag/C, which is in agreement with the kinetic data obtained by half-cell studies. APEMFC containing 0.5 mg$_{Ag}$/cm^2 of 60% Ag/C as cathode catalyst gives the maximum performance.

Acknowledgments Financial support from CSIR, New Delhi through a supra-institutional project under XI Five Year Plan is gratefully acknowledged. S. Maheswari is grateful to CSIR, New Delhi, for a Senior Research Fellowship.

References

1. M. Cifrain, K.V. Kordesch, J. Power Sources **127**, 234 (2004)
2. J.R. Varcoe, R.C.T. Slade, Fuel Cells **5**, 187 (2005)
3. J. O'M, S.S. Bockris, *Fuel cells: their electrochemistry* (McGraw-Hill, New York, 1969), p. 289
4. C.Y. Wu, P.W. Wu, P. Lin, Y.Y. Li, Y.M. Lin, J. Electrochem. Soc. **154**(10), B1059 (2007)
5. M.A. Kostowskyj, D.W. Kirk, S.J. Thrope, Int. J. Hydrogen Energy **35**, 5666 (2010)

6. L. Demarconnay, C. Coutanceau, J.-M. Léger, Electrochimica Acta **49**, 4513 (2004)
7. M.L. Chatenet, M. G-Bultel, R. Aurousseau, F. Durand, J. Andolfatto, Appl Electrochem **32**, 1131 (2002)
8. B.B. Blizana, P.N. Ross, N.M. Markovic, J Phys Chem B **110**, 4735 (2006)
9. A.E.S. Selighlome, J.R. Varcoe, A.R. Kucernak, J. Electrochem. Commun. **10**, 151 (2008)
10. F.W. Campbell, S.R. Belding, R. Baron, L. Xiao, R.G. Compton, J. Phys. Chem. C **113**, 9053 (2009)
11. C. Coutanceau, L. Demarconnay, C. Lamy, J.M. Léger, J. Power sources **156**, 14 (2006)
12. J.R. Varcoe, R.C.T. Slade, G.L. Wright, Y. Chen, J Phys Chem B **110**, 21041 (2006)
13. J.S. Park, S.H. Park, S.D. Yim, Y.G. Yoon, W.Y. Lee, C.S. Kim, J. Power Sources **178**, 620 (2008)
14. J-J. Han, N. Li, T. Zhang, J. Power Sources **193**, 885 (2009)
15. J. Guo, A. Hsu, D. Chu, R. Chen, J. Phys. Chem. C **114**(10), 4324 (2010)
16. G.K.H. Wiberg, K.J.J. Mayrhofer, M. Arenz, Fuel cells **10**, 575 (2010)
17. J. Zeng, J. Yeng, J. Lee, W. Shou, J Phys Chem B **110**, 24606 (2006)
18. S. Maheswari, G. Selvarani, P. Sridhar, S. Pitchumani, A.K. Shukla, ECS Trans. **33**(1), 1795 (2010)
19. S. Cheng, B. Wu, C. Cha, J. Electroanal. Chem. **416**, 53 (1996)
20. B.M. Jović, V.D. Jović, J. Serb. Chem. Soc. **69**(2), 153 (2004)
21. S. Grushevskaya, D. Kudryashov, A. Vvendenskii, Croatica chemica acta **81**(3), 467 (2008)
22. Y. Cheng, M. Yan, Z. Jiang, Electrochem. Solid-State Lett. **10**(3), F5 (2007)
23. F.H.B. Lima, J.F.R. de Castro, E.A. Ticianelli, J. Power Sources **161**, 806 (2006)
24. G.F. Alvarez, M. Mamlouk, K. Scott, Int. J. Electrochem. Sci. doi:10.4061/2011/684535
25. A. Habrioux, D. Diabaté, J. Rousseau, T.W. Napporn, K. Servat, L. Guétaz, A. Trokourey, K.B. Kokoh, Electrocatal **1**, 51 (2010)
26. W. Jen, H. Du, S. Zheng, H. Xu, Y. Zhang, J. Pyhs. Chem. B **114**, 6542 (2010)
27. K.E. Gubbins, R.D. Walker, J. Electrochem. Soc. **112**, 469 (1965)
28. R.R. Davis, G.L. Horvath, C.W. Tobias, Electrochim. Acta **12**, 287 (1967)
29. H. Meng, P.K. Shen, Electrochem. Commu. **8**, 588 (2006)
30. A.J. Bard, L.R. Faulkner, *Electrochemical methods* (Wiley, New Delhi, 2006), p. 341
31. J.S. Spendelow, A. Wieckowski, Phys Chem Chem Phys **9**, 2654 (2007)
32. C. Jeyabharathi, P. Venkateshkumar, J. Mathiyarasu, K.L.N. Phani, Electrochimica Acta **54**, 448 (2008)